International Journal on Interactive Design and Manufacturing (IJIDeM)
https://doi.org/10.1007/s12008-023-01506-2

ORIGINAL PAPER

Design and manufacturing of a hip joint motion simulator with a novel modular design approach

Shams Torabnia[1] · **Senay Mihcin**[2] · **Ismail Lazoglu**[1]

Received: 10 January 2023 / Accepted: 11 August 2023

Abstract
The study is aimed to develop a hip joint wear simulator using a modular design approach to help experimentally monitor and control critical wear parameters to validate in-silico wear models. The proper control and application of wear parameters such as the range of motion, and the applied force values while estimating the lost material due to wear are essential for thorough analysis of wear phenomena for artificial joints. The simulator's dynamics were first modeled, then dynamic loading data was used to calculate the forces, which were further used for topology optimization to reduce the forces acting on each joint. The reduction of the link weights, connected to the actuators, intends to improve the quality of motion transferred to the femoral head. The modular design approach enables topology-optimized geometry, associated gravitational and dynamic forces, resulting in a cost-effective, energy-efficient product. Moreover, this design allows integration of the subject specific data by allowing different boundary conditions following the requirements of industry 5.0. Overall, the in-vitro motion stimulations of the hip-joint prosthesis and the modular design approach used in the study might help improve the accuracy and the effectiveness of wear simulations, which could lead into the development of better and longer-lasting joint prostheses for all. The subject-specific and society-based daily life data implemented as boundary conditions enable inclusion of the personalized effects. Next, with the results of the simulator, CEN Workshop Agreement (CWA) application is intended to cover the personalized effects for previously excluded populations, providing solution to inclusive design for all.

Keywords Hip joint motion simulator · Multidisciplinary design · Modular design · Topology optimization · Industry 5.0

1 Introduction

Understanding the anatomy and mechanics of walking has been crucial in the design and development of artificial hip implants to improve the quality of life for patients with hip joint issues. Early studies by Carlet and Marey [1, 2], as well as Quénu and Demenÿ[3], provided initial insights into the forces acting on the hip during walking using measuring devices such as the dynamograph, which measured pressure differences between the heel and the forefoot. However, these early measurements were limited by the technology available at that time and were found to be not good enough in detail for designing hip implants [4, 5]. In recent years, technological advancements enabled accurate and detailed measurements methods for evaluation of the human gait cycles. Studies by Bergman et al. [6] have provided essential contributions in measuring different gait cycle patterns and understanding the relationship between the vertical reaction load and the body's acceleration center. These technological inputs, combined with engineering design principles, have improved the creation of artificial hip joints. Testing joint replacements is also critical in ensuring their fitness for the intended purpose. Advances in testing methods, such as finite element analysis (FEA) and biomechanical simulations [7], have allowed for better evaluation of the performance and durability of hip implants under various loading conditions, including those experienced during walking and other physical activities. This has led to the development more reliable and durable hip implants that can withstand the forces exerted during

✉ Senay Mihcin
senaymihcin@iyte.edu.tr

Shams Torabnia
STORABNIA19@KU.EDU.TR

Ismail Lazoglu
ilazoglu@ku.edu.tr

[1] Manufacturing, and Automation Research Center, Koç University, Istanbul, Turkey

[2] Department of Mechanical Engineering, Izmir Institute of Technology, Izmir, Turkey

Published online: 12 September 2023

daily activities, including walking and even more strenuous activities like running.

In vivo measurement of Total Hip Arthroplasty (THR) was performed by Rydell for the design of a total hip replacement [8] implanted with strain gauges to measure the gait cycle dynamically [9]. Since obtaining direct in vivo measurements from patients is problematic due to ethical issues, using simulators enables scientists to perform preclinical trials. In fact, as a part of the quality management chain, according to ISO-13485, it is necessary to maintain test setups to assure the quality of medical implants [10]. For this reason, the first in-vitro hip joint replacement simulator [11] was built. It was a machine with three degrees of freedom performing measurements. The later design [12] had a rotation around the flexion and extension axis. It could model vertical, and sidewalk loads since the designers believed the vertical load had a prominent role in walking. The third design was performed by Walker and Gold [13]. This design aimed to calculate the friction forces in the designed prostheses.

The significant problems in hip joint implants are the friction between the artificial femur head and the acetabular cup. The modeling of spherical joints has almost reached to maturity stage [14]. Wear and friction have become the primary concern in designing hip joint simulators [11]. In 2001, after a long debate between experts in hip implant surgery, manufacturing, and testing, a new ISO standard was introduced to cover all concerns of wear testing and wear test simulator requirements for total hip replacements [15]. ISO 14242 standard started to affect the design of recent preclinical joint simulators [16].

Among these simulators, the technique of estimating the wear on a femur head using coordinate measurement profilers was utilized [17]. While Trommer and Maru [18] designed their eight-station tester, Zanini et al. [19] used X-ray methodology to quantify wear. Partridge et al. [20] used a setup called Pro-sim, providing flexibility in both cup and femur holders. Viitala and Saikko [21] enabled improvements for the Helsinki University of Technology (HUT) simulators.

Although the first simulators aim for gait activities, regular walking is not the only daily life activity [22], since there are other daily life activities performed daily [23, 24]. With increase life of expectancy, today's patients want to continue their usual activities [25] without compromising their quality of life. The wear patterns and rates of joint prostheses may vary among populations with different religious and ethnic backgrounds due to their wider range of motions. This factor has been neglected in the past, and the study aims to investigate ways to provide quantitative evidence to address their unmet needs. Conversely, the populations with a limited range of motion, their needs have been met with the current standard implants. However, the investigation may lead to design changes for joint prostheses that will allow for higher ranges of motion and extended durability, which might benefit those populations without compromising their current quality standards. The proposed research can potentially eliminate the limitations of the current standard implants, enabling individuals to be more active and improve their quality of life. By providing quantitative evidence, the study can offer a more comprehensive understanding of wear patterns and wear rates among diverse populations, leading to better, more inclusive healthcare solutions. Ultimately, this can promote health equity by addressing the unmet needs of ethnic minority populations and allow them to access the same level of care as others. Ethical design philosophy requires producing products for all, without excluding minorities. For this reason, it is imperative to design and test implants according to their intended use. The testing conditions should cover these planned use activities as well.

The design of simulators for X (Design for a specific purpose) methods have been used for a long time, and the design methodologies focused on different emerging approaches every year [26]. Design for manufacturing, design for assembly [27], design for optimized workflow [28] and many other approaches are defined to create better products for different aspects. The main problem with many of these methods is that they were mostly trying to facilitate only one part of a product at a time, but they needed a comprehensive design approach. Also, since mass production is the main goal for many of these studies, the design of the test product has never been investigated deeply [29]. The primary purpose of creating a product is to fulfill a group of functions related to each other [30]. A detailed, comprehensive review of the literature shows that the design of a test machine needs a multidisciplinary method covering all aspects of the device.

This study demonstrates the design of a hip joint simulator mechanism that can perform flexion–extension (F/E), abduction–adduction (A/A), and internal–external rotation (I/E) to test the artificial hip joints in pre-clinical settings under dynamic loading at body temperature using simulated body fluid according to ISO 14242. Moreover, the machine design has the flexibility to simulate normal daily activities and some unique joint motions, such as stair climbing, praying, yoga postures, cycling, and any other personalized data to test the implant against its intended use. In this paper, the authors provide a methodology to design a simulator from concept to the prototype level with all the steps required to produce a custom-made simulator that can accept customized boundary conditions in addition to the standard boundary conditions of ISO 14242.

2 Design methodology

The design algorithm starts with design inputs. The conceptual design is in an iterative loop, so the concept matures

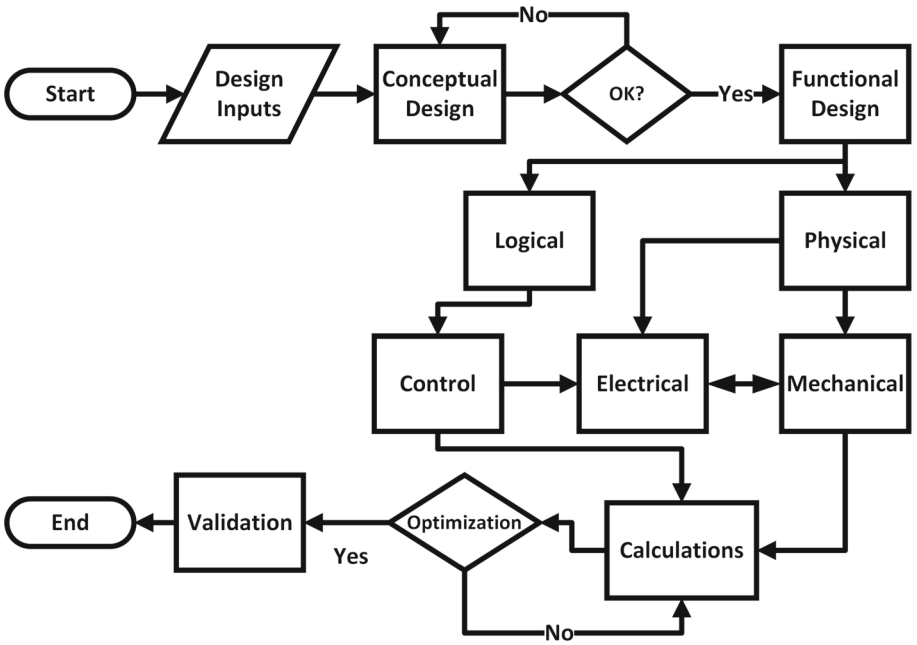

Fig. 1 The design algorithm proposed for the hip joint simulator demonstrating the decision points and the loops

up to serve the machine's purpose. The functional diagram of the device is generated based on the logic and physical properties of the system, such as mechanical parts, electrical parts, and their interaction. The system control is developed based on the functionality of the system and the mechanics modeled in CAD software. The electrical components are selected to serve both mechanics and controllability of the system. Then the design is optimized, and the results are sent for construction. The explained process is presented in Fig. 1.

The system's design requires an investigation of the interaction between different components. A modular design approach is proposed in this paper. This approach is potent enough to be implemented in all mechatronic systems. Figure 2 shows the graph presentation of the system interactions in the proposed model. The main idea is to define two main sub-trees for the physical domain, including all tangible items such as mechanical parts, wires, sensors, and the logical domain, covering functional aspects of the machine. The subsystems, α_i, β_i, ... provides a representation of the physical components as mentioned. Each logical parameter A_i, B_i, ... represents the system's local components. Such a point of view leads to a design structure matrix [31] helping prioritize the design based on need (such as design for X). The proposed model enables the creation of a multipurpose design by providing a visual comprehension of the system. Also, by having a correlation matrix of the function tree, the weightings of each interaction would be straightforward [32] in the design stage.

The hip joint motion simulator design has been performed and investigated using the proposed model.

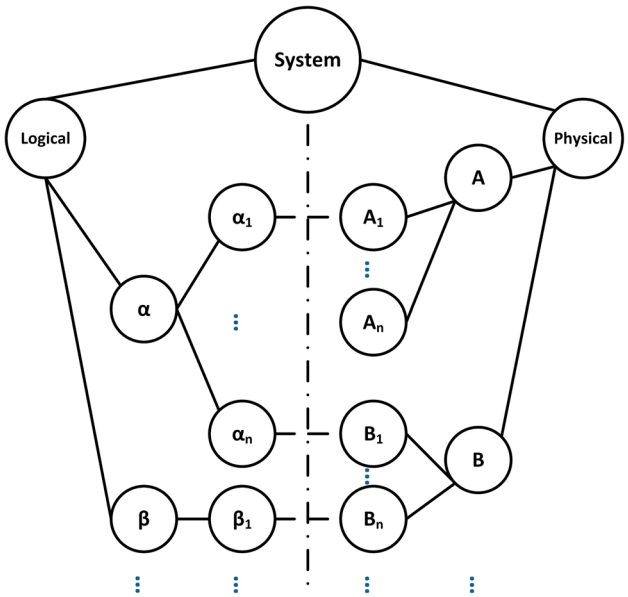

Fig. 2 The proposed functional model for the proposed product design

3 Hip joint motion simulator

3.1 Conceptual design

A comprehensive benchmarking has been performed to design this system. For such a range of motion, especially in Flexion–Extension, it is necessary to use a flexible mechanism [33, 34]. The benchmarking of the most critical designs is presented here. The values are compared with the standard values shown for the wear test of a femoral head [15]. The

Table 1 Benchmarking for Hip joint simulators available in market

	AMTI [35]	MTS [36]	Simulation Solutions [37]	ISO 14242 [38]
Axial loading (kN)	0–4.5	0–5.0	0–8.0	0–3.0
Loading from	Femoral Head	Femoral Head	Acetabular Cup	Acetabular Cup
Maximum cycle frequency (Hz)	2.0	1.0	2.5	1.0
Actuators	Servo Hydraulic	Servo Hydraulic	Servo Motor	–
Axes of motion	Non-Anatomical	Non-Anatomical	Strictly Anatomical	
Flexion–extension	± 100°	± 20°	± 60°	± 23°
Interior-exterior	± 40°	Not Disclosed	± 45°	± 12°
Abduction–adduction	± 25°	Not Disclosed	+ 10°/-25°	± 23°
Kinematic structure	P P R Table P R R(Spherical) Robotic Arm	R R R Table P load	R R R Table P load	R R R Table P load
Force actuation	Hydraulics	Hydraulics	Electromechanics	N/A
Motion actuation	Hydraulics	Electromechanics	Electromechanics	N/A

output of benchmarking is presented in Table 1. All these machines are trying to mimic the standard ranges according to ISO 14242. However, many activities require a higher range of motion. The products investigated are programmed to mimic the ISO standards and the custom-made motion profiles that could be programmed based on the subject-specific needs as an adaptation of Industry 5.0 evolution, including personalized specifications.

According to the literature [39] the femur hip range of motion could reach the following values. For Interior 112.1° ± 14.1° Exterior 43.2° ± 11.1° (I/E), Flexion 111.9° ± 8.9° Extension 49.8° ± 14.1° (F/E) and Abduction 46.1° ± 5.2° Adduction 61.0° ± 6.7° (A/A). The range of motion exceeds the values claimed by different designs. The primary intuition for designing a new simulator was to create a machine with a more flexible range of motion to cover personalized needs according to the requirements of Industry 5.0.

The newly designed simulator has a range of motion above all benchmarked products. The I/E range for this machine is -150° to + 150°, F/E ± 130°, and A/A range is ± 75°. This range covers the hip joint motion using the suitable fixture and possible range of motion for the Knee[40] and Ankle[41] joints. All motion and force actuation for this mechanism is electromechanical. Harmonic drive actuators [42] help decrease the weight of the actuators and integrate them into the robotic arm. The PC-based control system can program based on the motion trajectory needed. The general concept of the system was modeled in CAD software and then improved based on the structural analysis. The finalized concept of the machine is presented in Fig. 3. The machine consists of a fixed, rigid structure named as Frame in Fig. 3 holding the Base Tower Structure. The Base Tower Structure keeps the force mechanism aligned with the Trolley Assembly (shortened as Trolley Assy in Fig. 3) with a ball screw and two linear rails. Trolley Assy is the base for Abduction/Adduction(A/A) and Flexion/Extension(F/E) Arms applying load on the specimen. Beneath the specimen, a six-axis load cell reads the load, fixed on the rotary table which is actuated by another motor. The rotary table is assembled on a two-degree-of-freedom alignment table, to allow for mimicking the specimen's misalignments in the surgeries. The joint motion simulator follows the design modularity [43] is possible to change each motion module's design separately, as presented in the functional diagram (Fig. 4).

3.2 Functional design

Since this is an electromechanical system, the control side also plays a prominent role in the system's functioning. The functional diagram of the system is presented in Fig. 4. The interaction between the essential components is shown regarding the type of relation. Either it is a mechanical connection, a signal, or logical feedback. Load measurement is a closed feedback loop at the end effector that guarantees the system's calibration. As presented in Fig. 4, the feedback eliminates extra disturbances such as part deformations, zero-backlash actuators, and topology-optimized geometries, which secures the results.

Figure 5 shows the interactions between the system components. It also gives an idea of each system's function. The presented hierarchical correlation shows relations between different members of the sub-systems and gives an idea of how these different parts of the sub-system relate to each other. The fault detection analysis for the proposed model using the correlated features would be much easier than conventional models [44].

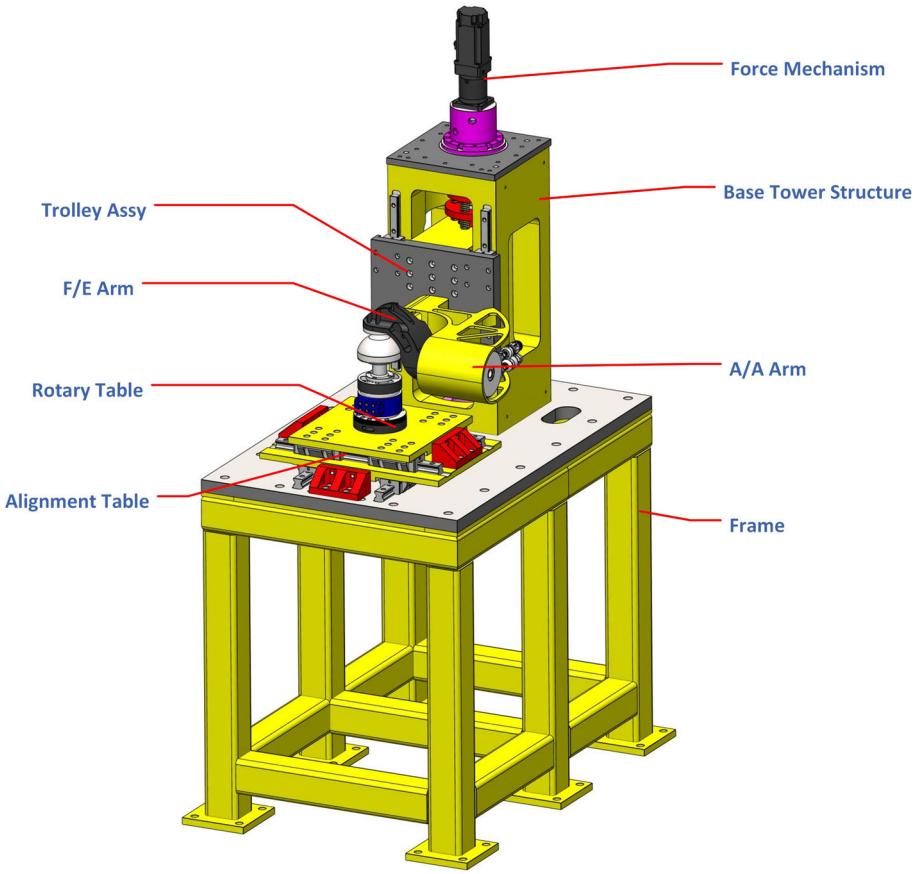

Fig. 3 The final concept of the hip joint motion simulator

3.3 Motion calculations

Arm axes consist of a wrist mechanism with three degrees of rotation. The force implication mechanism is intended not to cause any extra motions in the system's dynamics but to create only the desirable forces. The system dynamics for the acting arm are based on the free-body diagram, as shown in Fig. 6. The *q1* axis moves the A/A Arm. The second arm moves by the *q2* rotational motion moves F/E Arm. The *q3* is the motion for the rotary table, and *q4* is the linear motion applying force. The femoral head specimen is modeled as a spherical joint.

The system is considered a Prismatic-Rotation-Rotation-Rotation (PRRR) mechanism but is generally an RRR robot. The system transfer function can be calculated using the transfer functions for each joint regarding the {b} (the base) coordinate [45]. Joint 4 is the prismatic joint used for force implication. Therefore, this joint has no motion. The transformation is equal to the $\boldsymbol{I}_{4x4}$ matrix. The transformation matrix in SE3(the special Euclidean group of rigid body displacements in three dimensions) for each joint can be calculated by matrix multiplication [46].

$$H_1 = \begin{bmatrix} C_2C_3 & -S_3C_2 & S_2 & r \\ S_1S_2C_3 + S_3C_1 & -S_1S_2S_3 + C_1C_3 & -S_1C_2 & rC_1 - r \\ -S_2C_1C_3 + S_1S_3 & S_2S_3C_1 + S_1C_3 & C_1C_2 & rS_1 \\ 0 & 0 & 0 & 1 \end{bmatrix} \tag{1}$$

$$H_2 = \begin{bmatrix} C_2C_3 & -S_3C_2 & S_2 & 0 \\ S_3 & C_3 & 0 & r \\ -S_2C_3 & S_2S_3 & C_2 & 0 \\ 0 & 0 & 0 & 1 \end{bmatrix} \tag{2}$$

Equations 3 and 4 show the transformation matrices needed for force control. Using the definition of matrix exponential and Rodrigues's formula [46] for the force transformation later, a 6 × 6 matrix is formed, and the results are investigated. But before that, the systems' maximum speed and screws are identified. The rotational speed of the system is related to the force application frequency. According to the system's requirement, the hip implant's test frequency is 1 Hz.

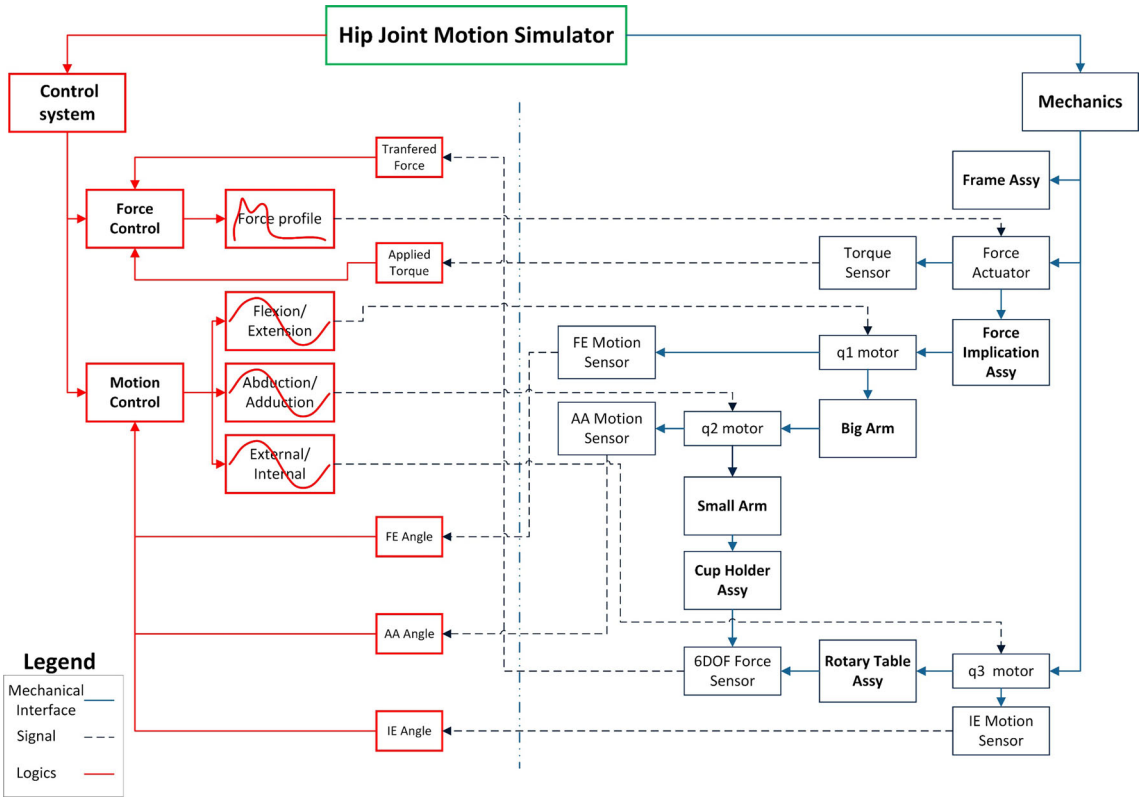

Fig. 4 The functional diagram of the simulator, blue line indicating the mechanical interface, the dashed line representing the signal, and the red representing the logics

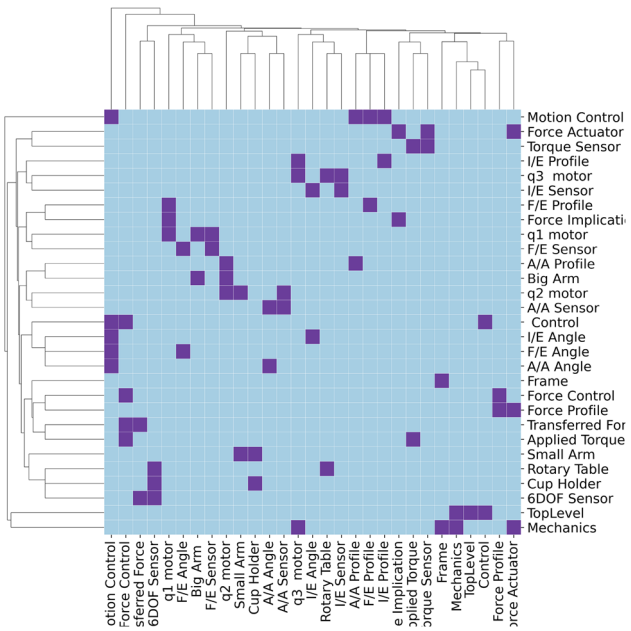

Fig. 5 Hierarchical correlation between different components

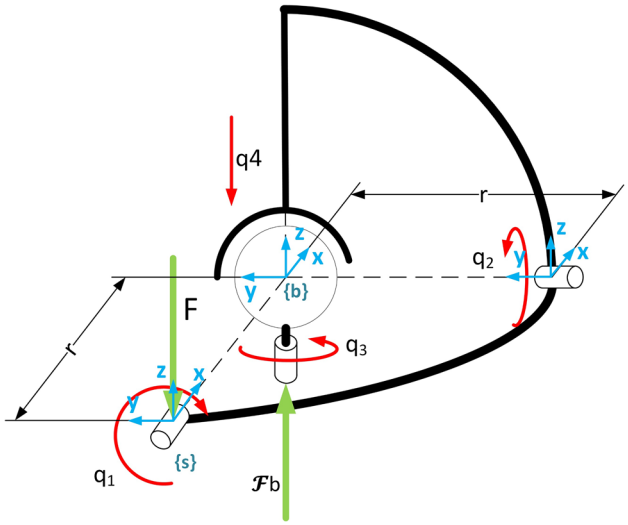

Fig. 6 A prismatic-rotation-rotation-rotation (PRRR) robotic arm used for the wear simulator

Therefore, by presenting screw vectors in the transformation from {b} coordinate to {s} could be rewritten as:

$$T(\theta) = e^{[\vec{s_4}]q_4} e^{[\vec{s_3}]q_3} e^{[\vec{s_2}]q_2} e^{[\vec{s_1}]q_1} M \tag{3}$$

Since there is no separation in the joint under test, term $e^{[\vec{s_4}]q_4}$ is equal to one, the screw vectors and transfer matrix for the end effector of the system are as follows:

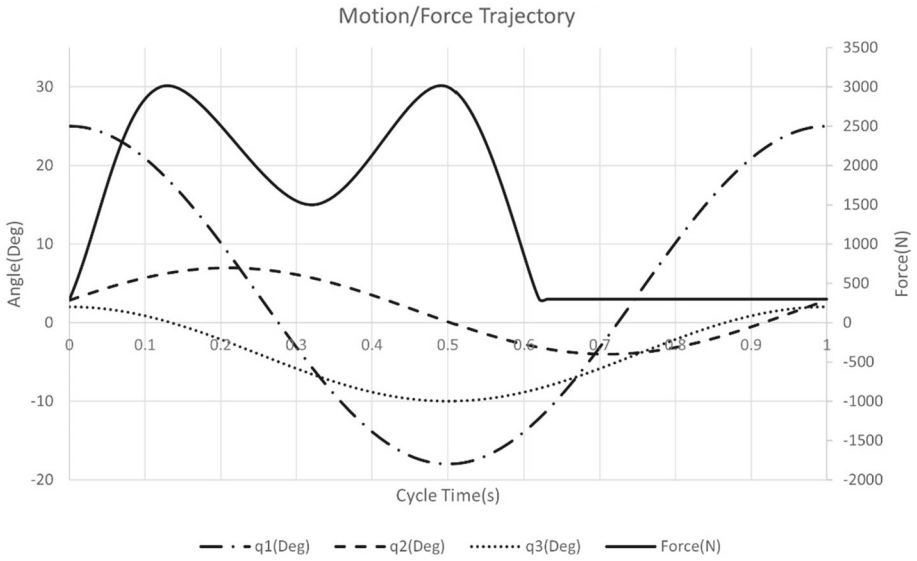

Fig. 7 Force versus joint angles motion for each cycle time(s)

$$\overrightarrow{s_1} = \begin{bmatrix} 1 \\ 0 \\ 0 \\ r \\ -r \\ 0 \end{bmatrix}; \overrightarrow{s_2} = \begin{bmatrix} 0 \\ 1 \\ 0 \\ 0 \\ r \\ 0 \end{bmatrix}; \overrightarrow{s_3} = \begin{bmatrix} 0 \\ 0 \\ 1 \\ 0 \\ 0 \\ 0 \end{bmatrix}; \overrightarrow{s_4} = \begin{bmatrix} 0 \\ 0 \\ 0 \\ 0 \\ 0 \\ 0 \end{bmatrix}; M = \begin{bmatrix} 1 & 0 & 0 & \mathrm{r} \\ 0 & 1 & 0 & 0 \\ 0 & 0 & 1 & 0 \\ 0 & 0 & 0 & 1 \end{bmatrix} \tag{4}$$

By defining the matrix adjoint, the translated force values are calculated [45].

$$[Ad_H] = \begin{bmatrix} R & 0 \\ -R^T[p] & R^T \end{bmatrix} \tag{5}$$

$$\mathcal{F}_b = [Ad_H]F \tag{6}$$

By defining the matrix adjoint, the translated force values are calculated [45]. Having the weights and the moments of inertias for the arms following forces on the joint are calculated using Eq. 7:

$$\mathcal{F}_n = \mathcal{G}_n\dot{\mathcal{V}}_n - \left[Ad_{\mathcal{V}_n}\right]^T\mathcal{G}_n\mathcal{V}_n \tag{7}$$

where $\mathcal{V}_b$ and $\dot{\mathcal{V}}_b$ are twists and their derivative (acceleration terms) of the bodies. b is the inertia matrix defined as follows.

is the moment of inertia matrix and $mI_{3\times3}$ is the multiplication of mass of the system by the diagonal one matrix.

Considering frictions and force components in the femur joint under the test, for the peak vales, force vector $_{\mathrm{b}}$ is assessed, and the force reactions are calculated using forward kinematics and Rodriguez formulation. These values aim to calculate the structural performance of the robot under dynamic conditions and the force/motion control loops.

Since the rotation motions of q1, q2, and q3 directly mimic the body motion, a look-up table based on the motion scenario applies to the system as in the robot path. This prevents any issues in three-dimensional altitudes, such as by positioning the arms in a position so that the mechanism eliminates one of its spherical degrees of freedom (gimbal lock). The force is synchronized with the motion output in each cycle. The implementation of the path for ISO 14242 is presented in Fig. 7.

All motion points regarding the control system are modelled by Simscape-Simulink (MATLAB, MathWorks, USA) are presented in Fig. 8. In this model, the friction forces of the femur joint are modelled as a 3D force. The results are compared to the final design.

3.4 Validation

The analysis has been performed on Adams, a multibody dynamics simulation tool (V2020, Hexagon, Stockholm, Sweden), to validate the models and formulations (Fig. 9). To run the validation case, the joint angles were specified according to ISO 14242 standards. A fixed force in the Y direction, equivalent to 3000 N is applied to the system. A periodic motion based on Fig. 7 is modelled on the system. This is the maximum force according to ISO 14242 standards. The joint reaction force in the *y* direction on the *q1* joint was selected for validation. The *q1* joint is where all

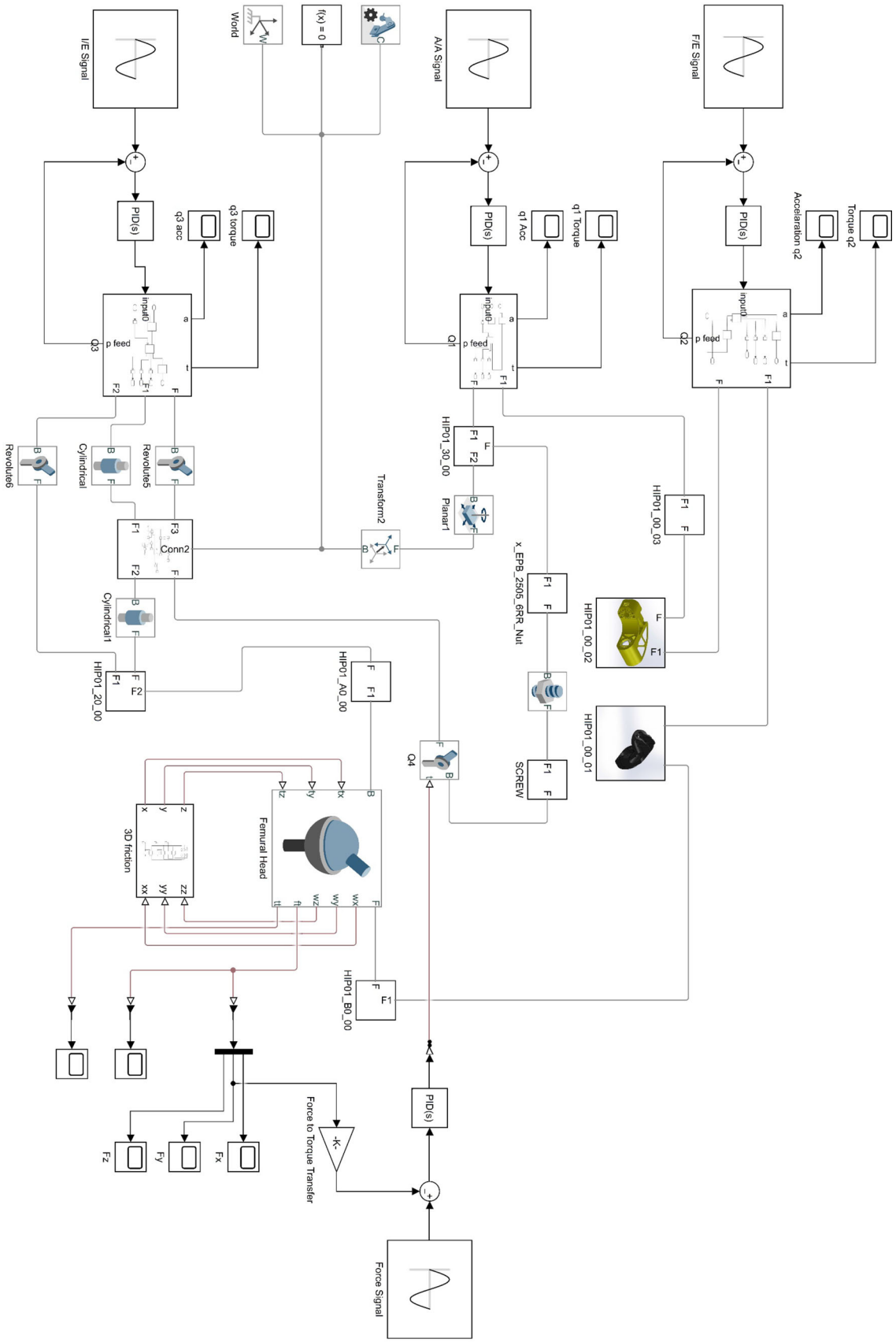

Fig. 8 The Simulink model for the hip motion simulator, including the frictional forces of the femur joint

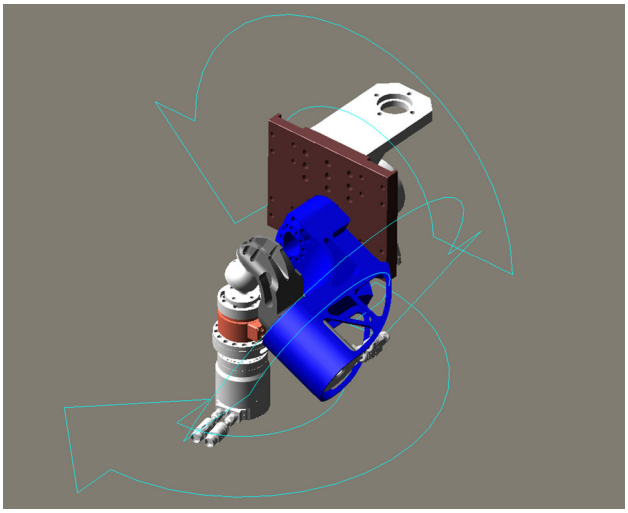

Fig. 9 The final design modeled in Adams, a multibody dynamic modeling software

joint forces are applied to the linear motion force mechanism (Fig. 3). The *Fy* component of the force is translated to the force mechanism through the linear guides and the ball screw.

The results from the Dynamic calculation were compared with the simulation results from Simulink and Adams (Fig. 10). The compared graphs show a difference of maximum 100 N between the Simscape and Adams models at the beginning and at the end of each period, which is about 4% of the instantaneous load. However, the dynamic model shows considerable difference. In the analytical model, all mass effects are neglected. Therefore, the mass-related equations of motion are equal to the zero. This will explain the discrepancy in the locations where maximum angular velocities occur in the periodic motion trajectory. The analysis conducted using Simscape and Adams' software exhibit better correlation, as both utilize rigid body modelling properties and dynamic equations. In contrast, the analytical model, which considers the mass matrix to be zero, may not accurately represent the physical behavior of the system.

4 Results and discussion

4.1 Force calculation results

Using Matrix adjoint in $\mathbb{R}^6$, by having force matrix, according to (5) and (6), (7) force calculations have been performed, and the reaction force for different rotation angles is plotted in Fig. 11 for the joint q1. The force values and their direction change according to the three different angles (*q1*, *q2*, *q3*) according to Fig. 6. The results are presented in Fig. 11.

Similarly, the force calculation was performed for joint *q2*. This joint rotates with the *A/A* Arm. The forces are related to joints *q2* and *q3* angles. Figure 12 represents the surface related to the force and moments' reaction on joint *q2*, similar to the analysis for joint *q1*.

The maximum and minimum forces for the end effectors transformed to each joint are calculated in Table 2. Therefore, the forces applied on joint three are equal to the force's values of frame $\{b\}(_b)$.

Based on the calculated forces, and since the motion is periodic, the structural calculations of the components were completed using this information.

4.2 Design optimization of robotic arms

For the robot arms, an arc shape design is considered to maintain the functionality and accessibility of the test specimen. A comprehensive performance investigation has been completed to understand whether the robot's arm geometry is optimized. According to the previous section, the loading condition was applied as a function of time, static/transient, and modal analysis. The results are presented in Fig. 13.

The findings indicate that even though both arms are capable of withstanding complete cyclic fatigue loading and

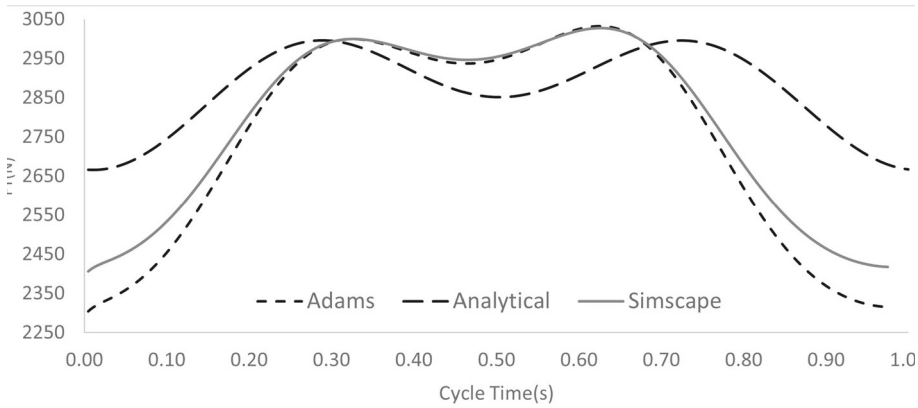

Fig. 10 Analytical model compared between Adams, Simscape for the Y-axis component of the force on q1 joint in a cycle time(s)

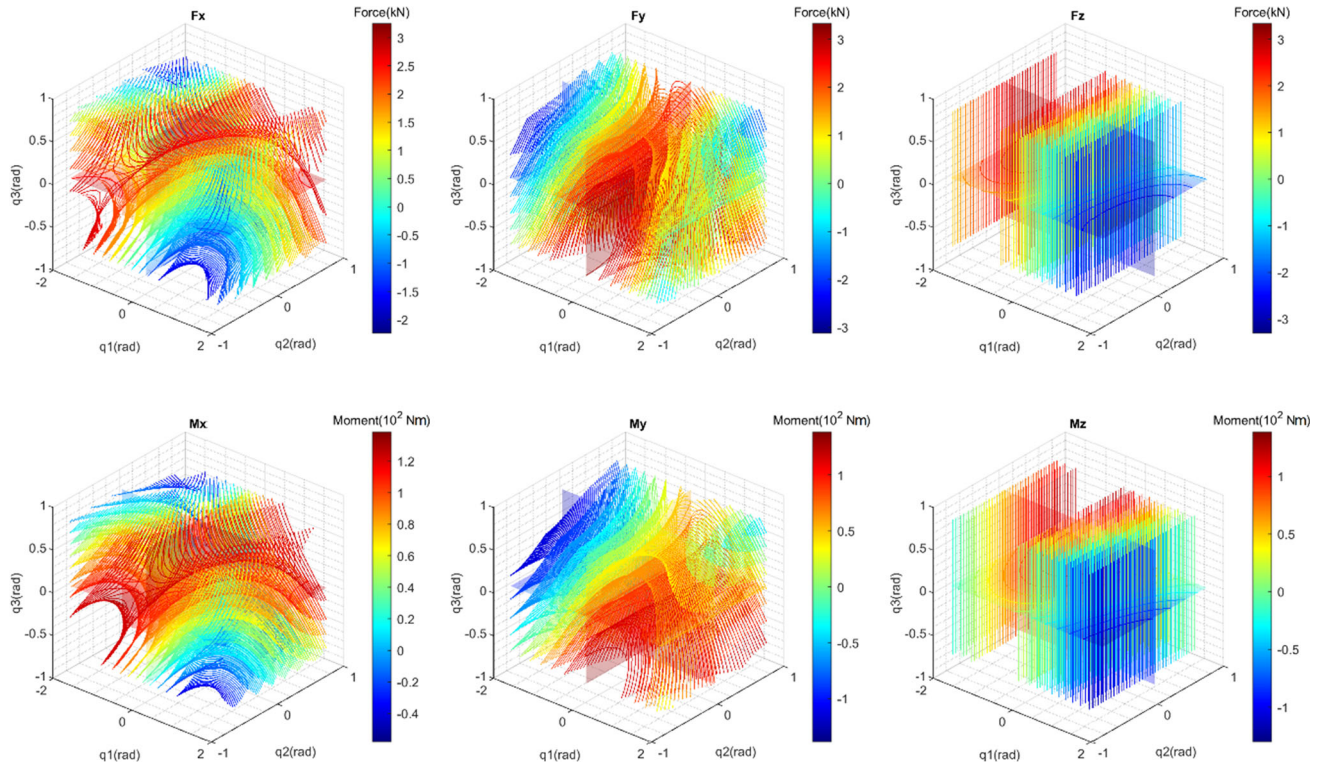

Fig. 11 q1 joint end-effector forces transformation

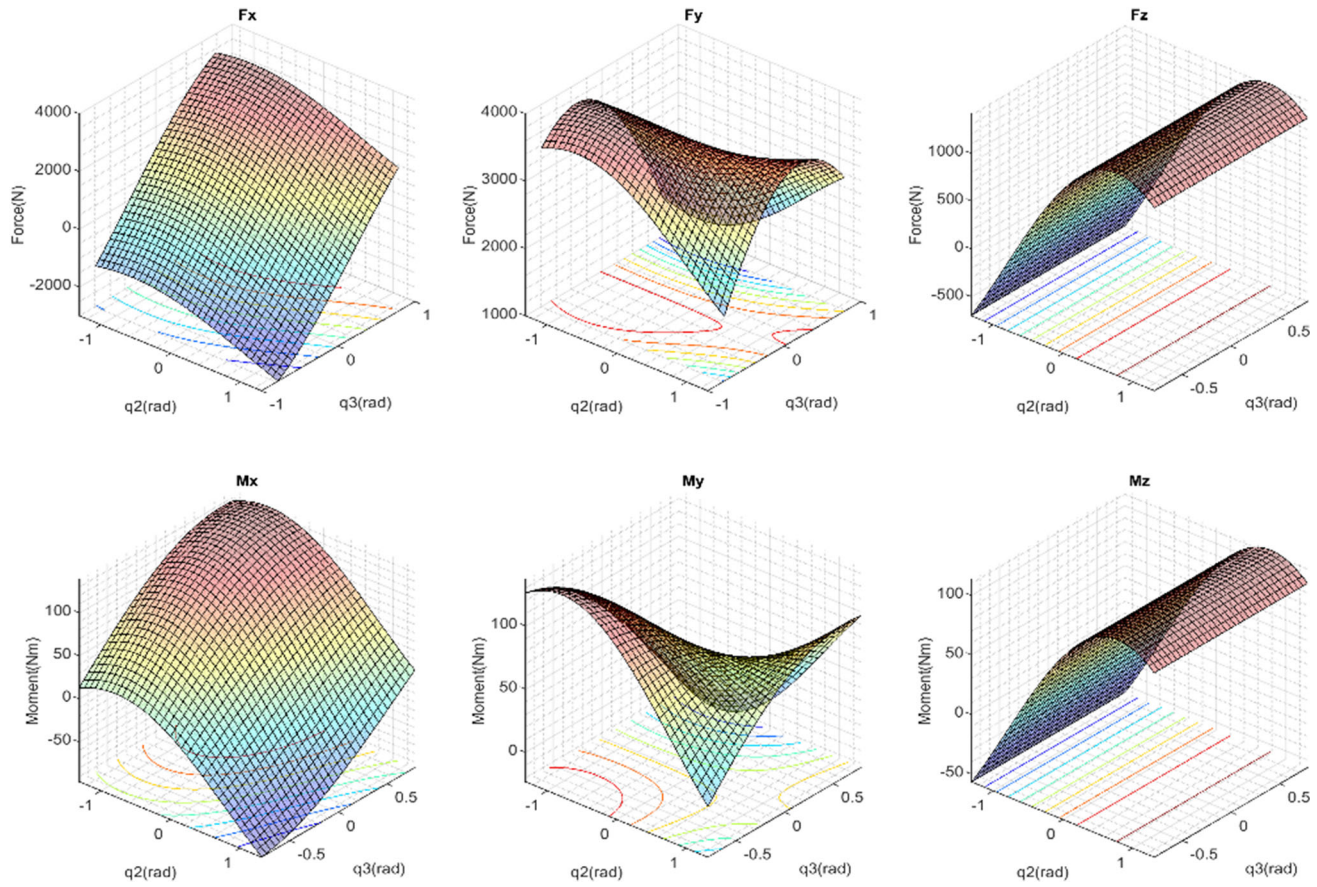

Fig. 12 q2 joint end-effector forces transformation

Table 2 Maximum values for the forces on joint q1 and q2 and q3

Joint	*Fx (N)*		*Fy (N)*		*Fz (N)*		*Mx (Nm)*		*My (Nm)*		*Mz (Nm)*	
	Max	Min	Max	Min	Max	Min	Max	Min	Max	Min	Max	Min
q1	3787	− 3409	3786	− 1091	3336	− 2048	139	− 97	139	− 98	139	− 78
q2	1964	− 1603	3769	2985	1415	− 692	85	13	130	68	114	− 58
q3	3500	− 3500	3500	− 3500	3500	− 3500	80	− 80	80	− 80	80	− 80

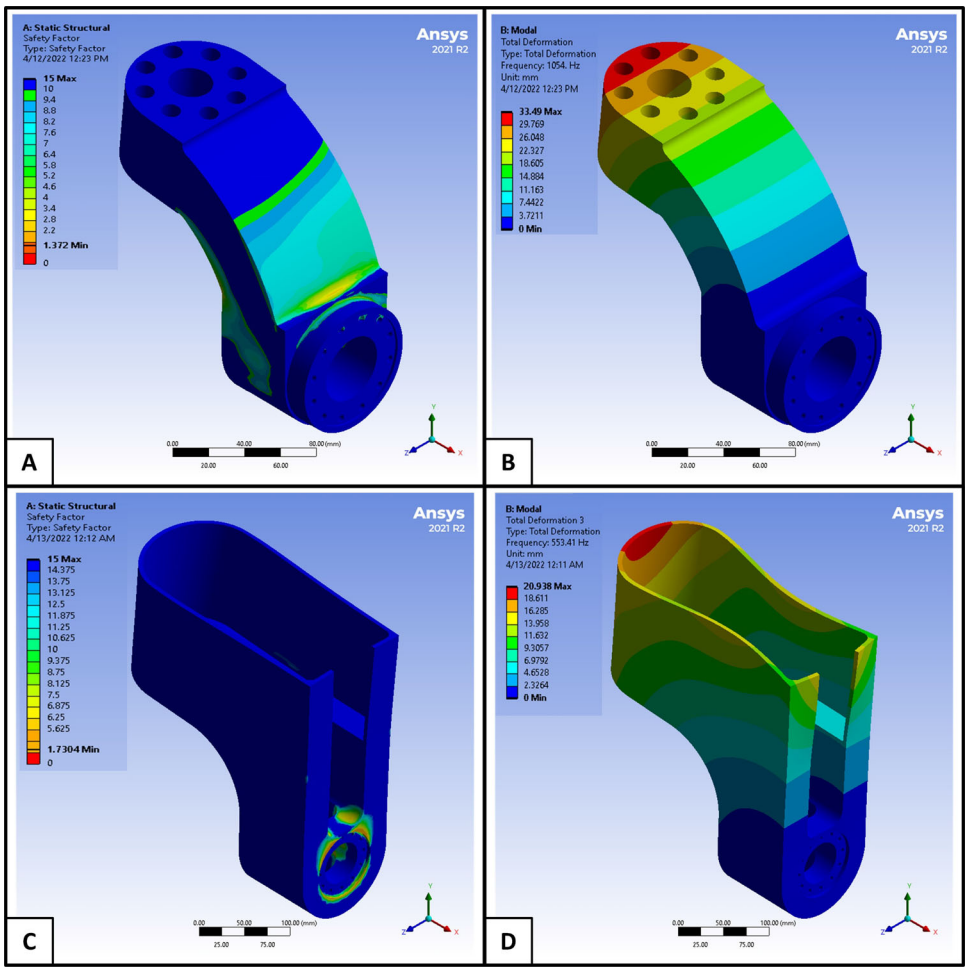

Fig. 13 F/E and A/A Arm Preliminary design fatigue safety factor (A, C) and first significant mode (B, D)

durable, there is still room for improvement in their optimization. The safety factor is calculated by dividing the yield stress by the equivalent fatigue stress occurring for a- full-cyclic load. Most design domains have a safety factor of more than 13. Usually, a safety factor of 1.1 to 1.5, would be enough for a robotic arm. For the *A/A* Arm, the first(409.3 Hz) and second (420.0 Hz) modal shape is related to the thin wall structure and cause insignificant bending or torsion. Therefore, the third modal shape is considered as a design reference point for comparison after topology optimization.

The Solid Isotropic Material Penalization (SIMP) topology optimization [47] has been applied to minimize the geometry's compliance and achieve the optimum mass. The main reason for mass optimization is to improve torques applied to the joints. By reducing the weights, the system's energy consumption is also optimized [48]. The size of the parts is about 500 × 500x200 for the *A/A* Arm and 150 × 150x100 for the *F/E* Arm. The selected material is St37-2 structural steel (with Young Modulus of 200GPa, Poisson ratio of 0.26, Yield Stress of 250 MPa, Density of 7860 kg/m^3) [49]. The design region and excluded region as well as objectives applied for topology optimization are presented in Fig. 14. The aim is to reduce the mass of the Arms. After a set of trials, and different mass reductions, the final

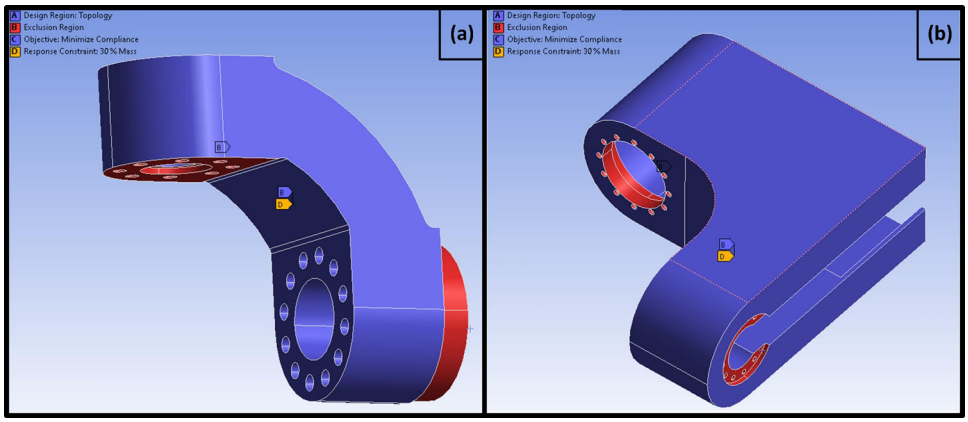

Fig. 14 Topology Optimization Design Region, Exclusions and Objectives for the F/E and A/A Arms

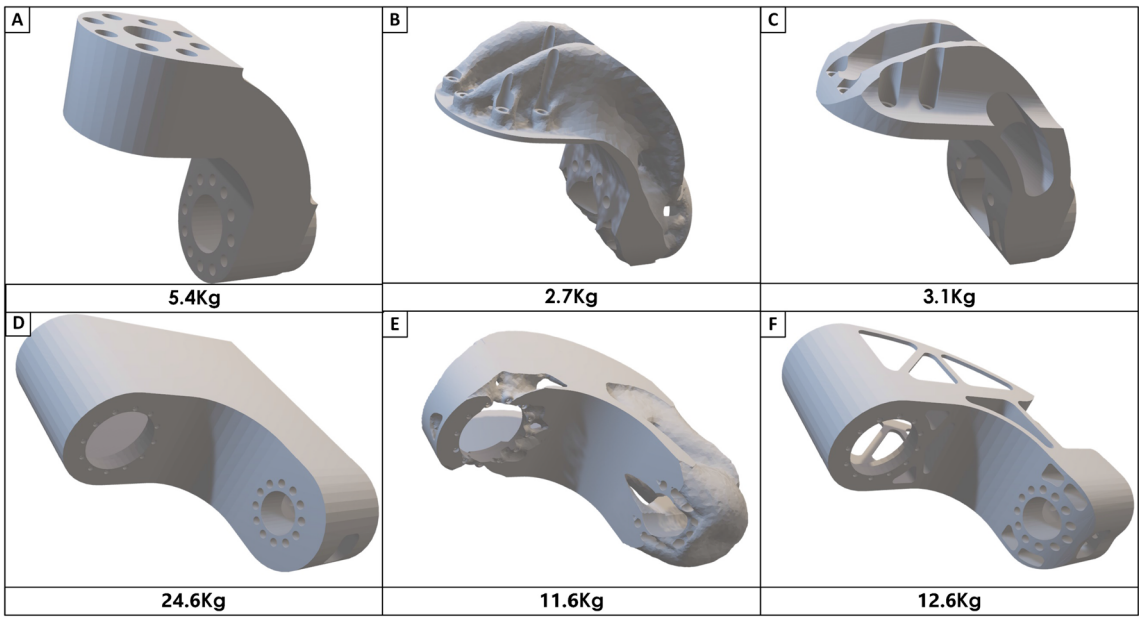

Fig. 15 Design optimization progress for F/E Arm (A, B, C) and A/A Arm (C, D, E)

Table 3 Results of Topology Optimization

	F/E Arm		A/A Arm	
Property	Concept	Optimized	Concept	Optimized
Weight (Kg)	5.4	3.1	24.6	12.6
Fatigue safety factor	1.50	1.43	1.73	1.63
Max deflection at the joint (mm)	0.042	0.066	0.043	0.076
Maximum stress (MPa)	62.83	68.47	49.81	52.58
First mode frequency	1054.4	1227.3	553.4(3^{rd})	725.8(5^{th})

design is set to have 30% of the original mass. The loading condition for this analysis is made according to the Fig. 7 and Table 2. The optimization has been performed, by applying maximum loading in each direction, considering the geometry is symmetric with respect to Plane A. The threshold to keep the removed mass is set as 0.4 during the trials.

Metal additive manufacturing methods like selective laser melting are expensive for this sort of dimensions. Using the geometry generated from topology optimization, a new geometry is modeled by removing any extra material from the preliminary design. The new design aims to be loyal to the topology optimized shape but with machinable features based on the authors' experience. Therefore, a new geometry

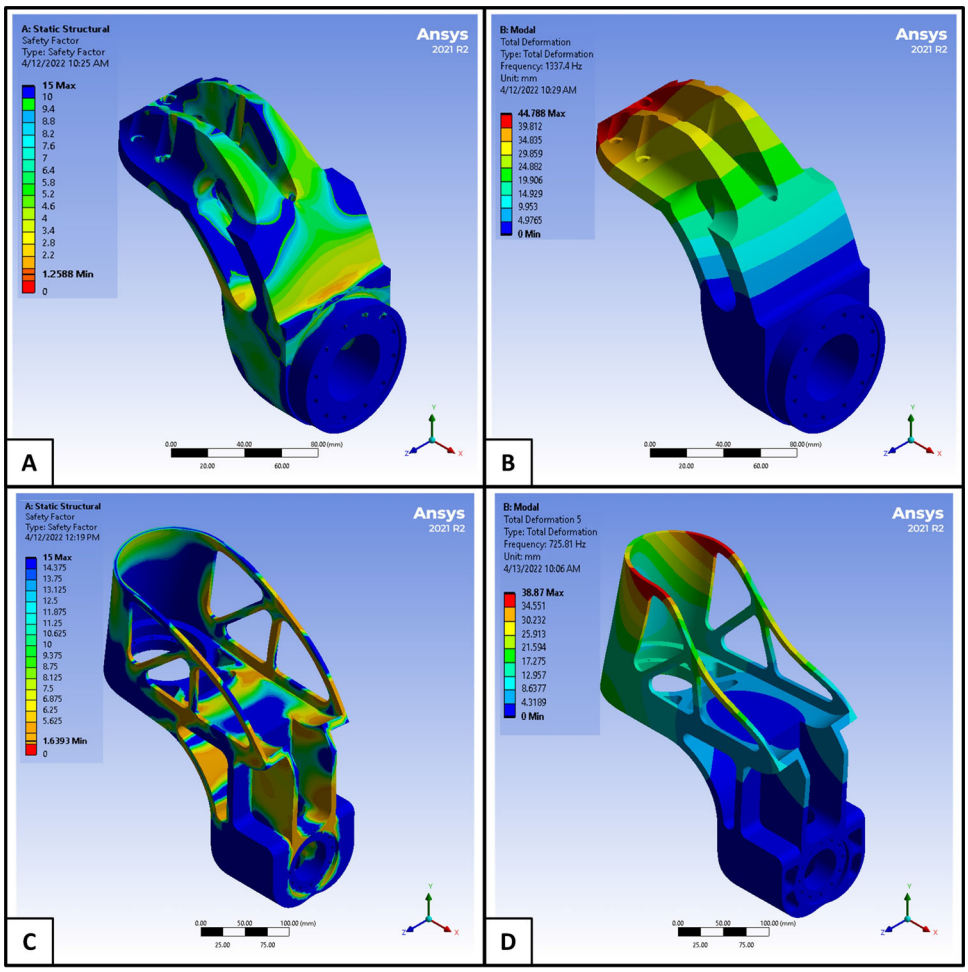

Fig. 16 F/E and A/A Arm Topology optimized design fatigue safety factor (A, C) and first significant mode (B, D)

is generated using topology optimization method to manufacture it using traditional manufacturing methods. The arms were manufactured via 5-axis CNC machine. The whole process for the *F/E* Arm and the *A/A* Arm are presented in Fig. 15, Table 3.

The topology-optimized inspired structure and mechanical performance were investigated by presenting the fatigue safety factor and the first significant mode in Fig. 16.

Since the required safety factor is about 1.5, it is essential to reduce the safety factor to prevent an over-designed structure and reduce the body mass. The safety factor for both arms shows that the blue areas, which have a safety factor of more than 15, could be reduced. The minimum safety factor of the system is set as 1.2 for F/E and 1.6 for A/A arms. The first mode shape of the F/E Arm increases by 26% compared to the original concept. This means that the structure has a lower tendency to bend for periodic motion. The main reason is better mass distribution in the design domain by minimizing the structure's compliance using topology optimization.

To understand the model analysis, the mode shapes for preliminary design and optimized shape are considered, and the mode shapes aligned with the loading condition are investigated. This means that the mode shapes related to local vibrations are omitted. For the A/A Arm, considering all mode shapes, the first mode decreased (343.6 Hz, 354.3 Hz, 392.7 Hz, 419.5 Hz), but these modes are related to the thin-walled structure generated by topology optimization. The first significant structure mode is the fifth mode and shows a 31% improvement.

To achieve optimal performance in a system's dynamic and control analysis, it is crucial to reduce its mass. The arms can be considered rigid if the system's first frequency is higher than the frequencies of external forces acting on it. It is important to note that the system operates at approximately 1 Hz. The first mode shapes of the arm are significantly higher than the excitation frequency before and after optimization.

The optimization result shows that although the strength of the arms is reduced and the safety factor for fatigue is decreased, the arms are still in the safe zone. The weight reduction has been performed to reduce the weight force values acting on the joints. The concept and topology-optimized design results are compared in Fig. 17. The force magnitude is diminished.

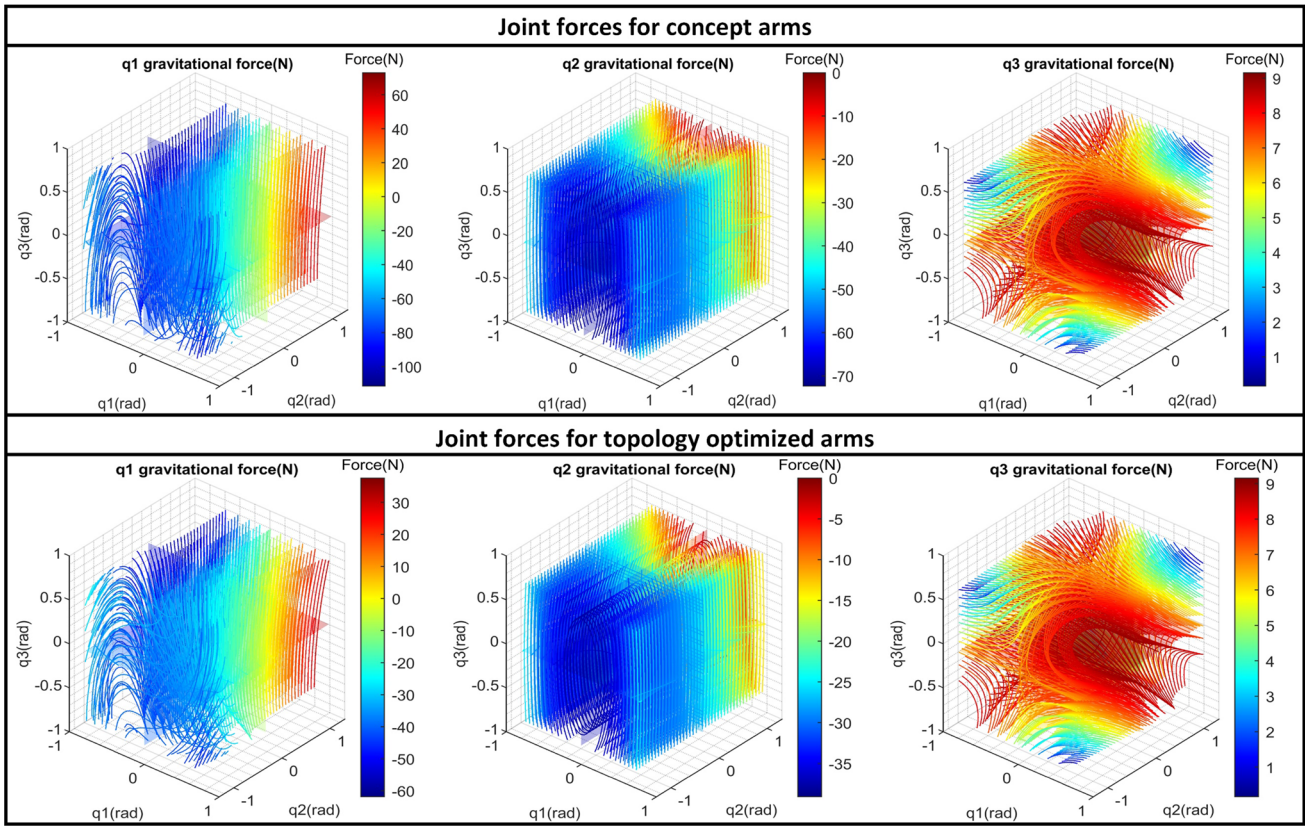

Fig. 17 The effect of the arm weights on the joints

The machine manufacturing is finalized, and there is ongoing research on implementing the control system and completing the test Fig. 18.

5 Conclusion

This study provides a comprehensive overview for the design of a hip joint simulator considering the multiple facets of the design process, including the control, energy efficiency, weight reduction, manufacturing aspects, and allowing different boundary condition applications following the requirements of Industry 5.0 for personalization. Now, such a comprehensive study exists in literature by this research. The work might tick the boxes for many design aspects due to the use of the modular approach used in this study.

The results show that using a Prismatic-Rotation-Rotation-Rotation PRRR robotic arm could make the load application mechanism more effective, and variety of force values could be covered. The effect of the weight of the arms on the joint is small. However, the topology optimization of the arms has been performed to have smoother test conditions. By means of the optimized topology shape, the effect of the arm weights on joint loading is decreased by about 55%. The optimized form was validated via FEM analysis, and the results show acceptable performance, compared to the original shape. Optimizing and generating the parts for the machining process have been performed for the first time for a simulator, which is intended to test medical devices according to ISO 13485 standards. As this robot performs a high number of cyclic loading tests (ten million cycles per specimen), this method could also be helpful for general robotic use, to minimize the weights of the robotic arms.

This paper provides a detailed step-by-step guide for designing a hip simulator and demonstrates the research process performed. The machine has completed its manufacturing, assembling, and wiring stages. Next, the test results for the device performance tests, verification, and validation algorithms are to be published in our subsequent publication.

With the manufacturing of this machine, by integrating the diverse daily life activities as boundary conditions for the wear tests, it will be possible to understand the wear mechanisms and wear limits for these activities. Based on the results of the wear tests over million cycle tests, CEN Workshop Agreement (CWA) application could be made to include diverse activity motion profiles for the previously excluded populations providing a solution to inclusive design for all motto as an addition to current standard ISO 14242 quality checks.

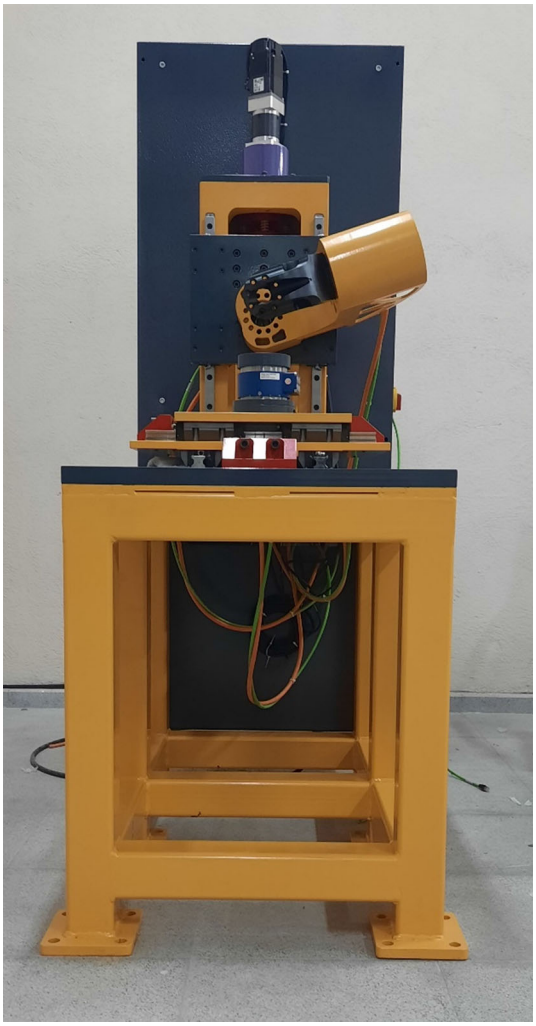

Fig. 18 The final manufactured and assembled hip simulator with completed wiring configuration and its electrical cabinet

Acknowledgements The authors thank the Manufacturing and Automation Research Center of Koc University for providing facilities for conducting the research jointly with the Mechanical Engineering Department of Izmir Institute of Technology.

Funding This research was funded by the TUBITAK 2232 International Outstanding Researchers Funding Scheme with Grant No of 118C188' New Generation Implants for All' project.

Declarations

Conflict of interest The authors declare that they have no competing interests.

Ethical Approval and Consent to Participate Not applicable.

Consent for Publication All authors give consent to the publication of this manuscript.

References

1. Carlet, G.: Essai expérimental sur la locomotion humaine : étude de la marche [Experimental test on human locomotion: Study of walking]. Impr. E. Martinet, Paris (1872)
2. Marey, É.J.: De la locomotion terrestre chez les bipèdes et les quadrupèdes [Terrestrial locomotion in bipeds and quadrupeds]. Impr. E. Martinet, Paris (1873)
3. Demenÿ, G., Quénu, É.A.V.A.: Etude de la locomotion humaine dans les cas pathologiques[Study of human locomotion in pathological cases]. Station Physiologique **4**, 1887–1889 (1888)
4. Uchida, T., Delp, S.: Biomechanics of Movement. The MIT Press, London, England (2020)
5. Shepherd, M.C., Gaffney, B.M.M., Song, K., Clohisy, J.C., Nepple, J.J., Harris, M.D.: Femoral version deformities alter joint reaction forces in dysplastic hips during gait. J. Biomech. **135**, 111023 (2022). https://doi.org/10.1016/J.JBIOMECH.2022.111023
6. Bergmann, G., et al.: Hip contact forces and gait patterns from routine activities. J. Biomech. **34**(7), 859–871 (2001). https://doi.org/10.1016/S0021-9290(01)00040-9
7. Aitken, H.D., Westermann, R.W., Bartschat, N.I., Clohisy, J.C., Willey, M.C., Goetz, J.E.: Effect of modeling femoral version and head-neck offset correction on computed contact mechanics in dysplastic hips treated with periacetabular osteotomy. J. Biomech. **141**, 111207 (2022). https://doi.org/10.1016/J.JBIOMECH.2022.111207
8. Rydell, N.W.: Forces acting on the femoral head-prosthesis. A study on strain gauge supplied prostheses in living persons. Acta Orthop. Scand. (1966). https://doi.org/10.3109/ort.1966.37.suppl-88.01
9. Ingelmark, B.E., Blomgren, E.: An apparatus for the measurement of pressure, especially in human joints. Upsala Lakareforen Forh. **53**(1–2), 75–94 (1948)
10. Mihcin, S., Ciklacandir, S., Kocak, M., Tosun, A.: Wearable motion capture system evaluation for biomechanical studies for hip joints. J. Biomech. Eng. (2021). https://doi.org/10.1115/1.4049199
11. Duff-barclay, B. I. and Spillman, D. T.: Total human hip joint prostheses—a laboratory study of friction and wear. vol. 181, no. 3 (1966)
12. Dowson, D., Walker, P.S., Longfield, M.D., Wright, V.: A joint simulating machine for load-bearing joints. Med. Biol. Eng. **8**(1), 37–43 (1970). https://doi.org/10.1007/BF02551747
13. Walker, P.S., Gold, B.L.: The tribology (friction, lubrication and wear) of all-metal artificial hip joints. Clin. Orthop. Relat. Res. **17**, 285–299 (1971). https://doi.org/10.1097/00003086-199608001-00002
14. Bai, S., Li, X., Angeles, J.: A review of spherical motion generation using either spherical parallel manipulators or spherical motors. Mech. Mach. Theory **140**, 377–388 (2019). https://doi.org/10.1016/J.MECHMACHTHEORY.2019.06.012
15. Kaddick, C., Wimmer, M.A.: Hip simulator wear testing according to the newly introduced standard ISO 14242. J. Biomech. **34**(SUPPL. 1), 429–442 (2001). https://doi.org/10.1016/s0021-9290(04)00168-x
16. Torabnia, S., Mihcin, S., and Lazoglu, I.: Parametric analysis for the design of hip joint replacement simulators. In: 2021 IEEE International Symposium on Medical Measurements and Applications (MeMeA), IEEE, Jun. 2021, pp. 1–6. doi: https://doi.org/10.1109/MeMeA52024.2021.9478689.
17. Tuke, M., Taylor, A., Roques, A., Maul, C.: 3D linear and volumetric wear measurement on artificial hip joints—validation of a new methodology. Precis. Eng. **34**(4), 777–783 (2010). https://doi.org/10.1016/j.precisioneng.2010.06.001

18. Trommer, R.M., Maru, M.M.: Importance of preclinical evaluation of wear in hip implant designs using simulator machines. Revista Brasileira de Ortopedia (English Edition) **52**(3), 251–259 (2017). https://doi.org/10.1016/j.rboe.2016.07.004
19. Zanini, F., Carmignato, S., Savio, E., Affatato, S.: Uncertainty determination for X-ray computed tomography wear assessment of polyethylene hip joint prostheses. Precis. Eng. **52**, 477–483 (2018). https://doi.org/10.1016/j.precisioneng.2018.02.009
20. Partridge, S., Tipper, J.L., Al-Hajjar, M., Isaac, G.H., Fisher, J., Williams, S.: Evaluation of a new methodology to simulate damage and wear of polyethylene hip replacements subjected to edge loading in hip simulator testing. J. Biomed. Mater. Res. B Appl. Biomater. **106**(4), 1456–1462 (2018). https://doi.org/10.1002/jbm.b.33951
21. Viitala, R., Saikko, V.: Effect of random variation of input and various daily activities on wear in a hip joint simulator. J. Biomech. **106**, 1–7 (2020). https://doi.org/10.1016/j.jbiomech.2020.109831
22. Safartoobi, M., Dardel, M., Daniali, H.M.: Gait cycles of passive walking biped robot model with flexible legs. Mech. Mach. Theory **159**, 104292 (2021). https://doi.org/10.1016/J.MECHMACHTHEORY.2021.104292
23. Lunn, D.E., Chapman, G.J., Redmond, A.C.: Hip kinematics and kinetics in total hip replacement patients stratified by age and functional capacity. J. Biomech. **87**, 19–27 (2019). https://doi.org/10.1016/j.jbiomech.2019.02.002
24. Sriramdas, R., Cruz, R., Garcia, A.J., Sharpes, N.L., Priya, S.: Human gait energy harvesting through decoupled suspended load backpacks. Mech. Mach. Theory **171**, 1047 (2022). https://doi.org/10.1016/J.MECHMACHTHEORY.2022.104734
25. Srivastava, G., Christian, N., Fred Higgs, C.: A predictive framework of the tribological impact of physical activities on metal-on-plastic hip implants. Biotribology (2021). https://doi.org/10.1016/j.biotri.2020.100156
26. Watson, B., Radcliffe, D., and Dale, P.: A meta-methodology for the application of DFX design guidelines. In: Design for X, Dordrecht: Springer Netherlands, pp. 441–462 (1996)
27. Formentini, G., Bouissiere, F., Cuiller, C., Dereux, P.-E., Favi, C.: Conceptual design for assembly methodology formalization: systems installation analysis and manufacturing information integration in the design and development of aircraft architectures. J. Ind. Inf. Integr. **26**, 100327 (2022). https://doi.org/10.1016/j.jii.2022.100327
28. George, A., Ali, M., Papakostas, N.: Utilising robotic process automation technologies for streamlining the additive manufacturing design workflow. CIRP Ann. **70**(1), 119–122 (2021). https://doi.org/10.1016/j.cirp.2021.04.017
29. Huang, G.Q., Lee, S.W., Mak, K.L.: Web-based product and process data modelling in concurrent 'design for X.' Robot. Comput. Integr. Manuf. **15**(1), 53–63 (1999). https://doi.org/10.1016/S0736-5845(98)00028-3
30. Mcharek, M., Hammadi, M., Azib, T., Larouci, C., Choley, J.-Y.: Collaborative design process and product knowledge methodology for mechatronic systems. Comput. Ind. **105**, 213–228 (2019). https://doi.org/10.1016/j.compind.2018.12.008
31. Buzuku, S., Kraslawski, A.: Use of design structure matrix for analysis of critical barriers in implementing eco-design initiatives in the pulp and paper Industry. Proc. Manuf. **11**, 742–750 (2017). https://doi.org/10.1016/j.promfg.2017.07.175
32. van Beek, T.J., Erden, M.S., Tomiyama, T.: Modular design of mechatronic systems with function modeling. Mechatronics **20**(8), 850–863 (2010). https://doi.org/10.1016/j.mechatronics.2010.02.002
33. Ungethüm, M., Hildebrandt, J., Jäger, M., Moslé, H.G.: Ein neuer Simulator zur Testung von Totalendoprothesen für das Hüftgelenk. Arch. Orthop. Unfallchir. **77**(4), 304–314 (1973). https://doi.org/10.1007/BF00418916
34. Shan, X., Cheng, G.: Structural error and friction compensation control of a 2(3PUS + S) parallel manipulator. Mech. Mach. Theory **124**, 92–103 (2018). https://doi.org/10.1016/J.MECHMACHTHEORY.2018.02.004
35. Haider, H., Weisenburger, J.N., Garvin, K.L.: Simultaneous measurement of friction and wear in hip simulators. Proc. Inst. Mech. Eng. H **230**(5), 373–388 (2016). https://doi.org/10.1177/0954411916644476
36. Sonntag, R., et al.: Friction in hip bearings under continuous normal walking conditions: influence of swing phase load and patient weight. Biotribology (2021). https://doi.org/10.1016/j.biotri.2021.100182
37. Ali, M., Al-Hajjar, M., Partridge, S., Williams, S., Fisher, J., Jennings, L.M.: Influence of hip joint simulator design and mechanics on the wear and creep of metal-on-polyethylene bearings. Proc Inst Mech Eng H **230**(5), 389–397 (2016). https://doi.org/10.1177/0954411915620454
38. ISO/TC 150/SC 4 Bone and joint replacements comittee, ISO 14242–1:2014 Implants for surgery—wear of total hip-joint prostheses—Part 1 Loading and displacement parameters for wear-testing machines and corresponding environmental conditions for test," 2014.
39. Zhang, J., Wei, J., Mao, Y., Li, H., Xie, Y., Zhu, Z.: Range of hip joint motion in developmental dysplasia of the hip patients following total hip arthroplasty with the surgical technique using the concept of combined anteversion: a study of Crowe I and II patients. J. Arthroplasty **30**(12), 2248–2255 (2015). https://doi.org/10.1016/j.arth.2015.06.056
40. Stephens, J.D., Hurst, J.M., Morris, M.J., Berend, K.R., Lombardi, A.V., Crawford, D.A.: Correlation between patient-reported 'happiness' with knee range of motion and objective measurements in primary knee arthroplasty. J. Arthroplasty (2022). https://doi.org/10.1016/j.arth.2022.01.037
41. Usuelli, F.G., Indino, C., Leardini, A., Manzi, L., Ortolani, M., Caravaggi, P.: Range of motion of foot joints following total ankle replacement and subtalar fusion. Foot Ankle Surg. **27**(2), 150–155 (2021). https://doi.org/10.1016/j.fas.2020.03.015
42. Dong, H., Dong, B., Zhang, C., Wang, D.: An equivalent mechanism model for kinematic accuracy analysis of harmonic drive. Mech. Mach. Theory **173**, 104825 (2022). https://doi.org/10.1016/J.MECHMACHTHEORY.2022.104825
43. Kim, K., Kim, J., Kim, J., Kim, H.S., Kim, J.: Multidisciplinary methodology to predict the performance of modular actuator-based manipulator. Robot. Comput. Integr. Manuf. **52**, 46–64 (2018). https://doi.org/10.1016/j.rcim.2018.02.007
44. Manka, M., Uhl, T.: Mechatronic design of fault detection isolation and restoration systems for rotating machineries. Mech. Mach. Theory **44**(7), 1436–1449 (2009). https://doi.org/10.1016/j.mechmachtheory.2008.11.011
45. Lynch, K.M., Park, F.C.: Modern Robotics Mechanics, Planning, and Control, 1st edn. Cambridge University Press, Cambridge (2017)
46. Dai, J.S.: Euler–Rodrigues formula variations, quaternion conjugation and intrinsic connections. Mech. Mach. Theory **92**, 144–152 (2015). https://doi.org/10.1016/J.MECHMACHTHEORY.2015.03.004

47. Bendsøe, M.P., Sigmund, O.: Topology Optimization. Springer, Berlin (2004)
48. Carabin, G., Wehrle, E., Vidoni, R.: A review on energy-saving optimization methods for robotic and automatic systems. Robotics (2017). https://doi.org/10.3390/robotics6040039
49. Bauccio, M.: ASM Metals Reference Book. ASM International, Materials Park, OH (1993)